Hyperbolicity and change of type in flows of FENE-P fluids

B.Purnode V.Legat *

Université Catholique de Louvain, Cesame, Applied Mechanics,
4 avenue G. Lemaître, 1348-Louvain-la-Neuve, BELGIUM.

Abstract

In 1986, Dupret and Marchal [1] determined two tensorial conditions in order to analyze the loss of evolution and the change of type for Maxwell fluid flows. We perform here a quasi-linear analysis of the characteristics in flows of FENE-P fluids. Mathematical and easily computable conditions have been derived and can be used as criteria in complex flows. A similar result is also available for the Chilcott-Rallison model. The change of type is analyzed for flows through an abrupt contraction. Numerical results show that the vortex enhancement mechanism may be coupled with the change of type. A numerical simulation of the tree-like jet flow has also been performed.

*Université Catholique de Louvain Applied Mechanics (CESAME) 4 av. G Lemaître, B-1348 Louvain-la-Neuve BELGIUM

1 Introduction

In 1986, Dupret and Marchal [1] presented a general study of the characteristics in three dimensional flows of a Maxwell-B fluid. They determined a tensorial criterion that guarantees the evolutionary character of the equations. In the case of a steady flow, the problem is neither purely elliptic nor purely hyperbolic. However, the hyperbolic character of the flow can change. This has been called a *change of type* by Joseph *et al.* [2]. Dupret and Marchal [1] determined a general condition governing the change of type to a hyperbolic supercritical regime.

In this paper, we extend the approach of Dupret and Marchal [1] to the case of a FENE-P fluid. An evolution condition and a criterion governing the change of type for the stationary problem are presented in tensorial form. In limiting cases, it is shown that the conditions reduce to those of a Mawell-B fluid.

We then analyze numerically the change of type for flows through contraction and expansion geometries. The calculations are mainly done with a Galerkin formulation of the mixed finite element introduced by Marchal and Crochet [3] which allows to simulate flows with strong interaction between viscoelasticity and inertia. We are first considering the simulation of flows of a 0.25% polyacrylamide aqueous solution through a 4:1 abrupt contraction described in Purnode and Crochet [4]. This study was based on the experimental observations of Evans and Walters [5] for low concentrated polyacrylamide aqueous solutions. The FENE-P model is used to describe the rheological behaviour of the polymer solution. Numerical simulation allows us to show that the vortex enhancement mechanism may be coupled with the change of type. We then wish to simulate the *tree-like jet* flow observed experimentally by Giesekus [6] when a fluid flows from a circular hole into a large reservoir. Giesekus [6] notes that this effect occurs beyond a critical speed of the fluid, just as the delayed die swell. Using the same fluid data as for the 4:1 contraction case and for some specific values of the flow parameters, we show that the tree-like jet flow is associated with the change of type of the governing set of equations.

In section 2, we recall the basic equations of the differential viscoelastic models. We then briefly present the FENE-P model and we introduce the generic block-tensor notation of the problem. In section 3, we present the quasi-linear analysis for the determination of the characteristic sheets and we derive two tensorial conditions. Finally, in section 4, we present numerical simulations of the flows through contraction and the expansion geometries.

2 Basic Equations and Notations

2.1 Differential Viscoelastic Models

For incompressible fluids, the conservation laws of momentum and mass yield the following equations

$$\begin{aligned} \boldsymbol{\nabla}\cdot\boldsymbol{T}-\boldsymbol{\nabla}p+\boldsymbol{f} &= \rho\frac{D\boldsymbol{v}}{Dt}, \\ \boldsymbol{\nabla}\cdot\boldsymbol{v} &= 0. \end{aligned} \tag{1}$$

Here, $\boldsymbol{v}$ is the velocity vector, $\boldsymbol{T}$ the extra-stress tensor, p the pressure, $\boldsymbol{I}$ the unit tensor, $\boldsymbol{f}$ the body force per unit volume of fluid and ρ the fluid density. The operator D/Dt denotes the material time derivative.

The set of governing equations (1) is closed by a constitutive relationship that relates the extra-stresses $\boldsymbol{T}$ to the kinematic tensors. First, we often identify the presence of a purely-viscous component which may be interpreted as the solvent contribution to the stress in polymeric solution or as the stress response associated with a very fast relaxation mode. Therefore, we can split the tensor $\boldsymbol{T}$ as follows

$$\boldsymbol{T} = \boldsymbol{T}_N+\boldsymbol{T}_V,$$

where $\boldsymbol{T}_N$ is the Newtonian component and $\boldsymbol{T}_V$ denotes the viscoelastic extra-stress.

- On one hand, the Newtonian component is characterized by

$$\begin{aligned} \boldsymbol{T}_N &= 2\eta_N\boldsymbol{D}, \\ \boldsymbol{D} &= \left(\frac{\boldsymbol{\nabla v}+\boldsymbol{\nabla v}^T}{2}\right), \end{aligned}$$

  where η_N is the so-called Newtonian viscosity, and $\boldsymbol{D}$ is the rate-of-deformation tensor.

- On the other hand, let us now consider the simplest and most popular differential constitutive equation for $\boldsymbol{T}_V$:

$$\boldsymbol{T}+\lambda\overset{\triangledown}{\boldsymbol{T}}_V=2\,\eta_V\boldsymbol{D}. \tag{2}$$

  Here, λ is the relaxation time and η_V is the viscoelastic viscosity coefficient. The operator $\triangledown$ stands for the upper-convected derivative :

$$\overset{\triangledown}{\boldsymbol{T}}_V = \frac{D\boldsymbol{T}_V}{Dt}-\boldsymbol{T}_V\cdot\boldsymbol{\nabla v}-\boldsymbol{\nabla v}^T\cdot\boldsymbol{T}_V.$$

Depending on the occurence or not of a Newtonian component T_N, such a constitutive viscoelastic equation characterizes an Oldroyd-B or an upper-convected Maxwell model.

In a Oldroyd-B model, the retardation time is defined by

$$\lambda^* = \lambda \frac{\eta_N}{(\eta_N + \eta_V)}.$$

In the case of a vanishing Newtonian extra-stress component T_N, Dupret and Marchal [1] defined the tensor $\boldsymbol{T}_A$ as:

$$\boldsymbol{T}_A = \boldsymbol{T}_V + \frac{\eta_V}{\lambda}\boldsymbol{I} \tag{3}$$

and showed that in the case of a Maxwell-B flow problem with well-defined boundary conditions, the set of governing equations is no longer evolutionary where $\boldsymbol{T}_A$ is non positive-definite. When inertia is taken into account in the steady-state problem, the vorticity equation changes from elliptic to hyperbolic type as the tensor $\boldsymbol{T}_B$ defined by:

$$\boldsymbol{T}_B = \boldsymbol{T}_A - \rho \boldsymbol{v}\boldsymbol{v}, \tag{4}$$

loses its positive definiteness [2].

2.2 The FENE-P Model

However, these models do not provide a realistic description of polymeric fluids. As a mathematical model, the Finitely-Extensible-Non-Linear-Elastic-Dumbbell (FENE) equation appears to be a reasonable compromise between simplicity and physical reality.

Let us briefly recall the origin of the FENE model. The polymer macromolecules are considered as dumbbells suspended in a Newtonian solvent of a given viscosity η_N. Assuming that the solvent contribution is identified by $\boldsymbol{T}_N$, this theory leads to the following expression for the viscoelastic extra-stress tensor [7] [8].

$$\boldsymbol{T}_V \;=\; n < F(R)\; \boldsymbol{R}\boldsymbol{R} > -nkT\boldsymbol{I}, \tag{5}$$

where the stress caused by the Brownian motion is characterized by $-nkT\boldsymbol{I}$ where n is the number of dumbbells per unit volume, T is the temperature and k the Boltzmann constant. Finally, the term $n < F(R)\; \boldsymbol{R}\boldsymbol{R} >$ is the contribution from the tension $F(R)\; \boldsymbol{R}$ in the connectors. The brackets indicate an average over the distribution and $\boldsymbol{R}$ is the end-to-end vector for the dumbbells. In particular, the function F characterizes the amplitude of the connector force as a function of the length R of the vector $\boldsymbol{R}$.

The kinetic theory assumes that the motion of dumbbells is the result of the hydrodynamic force, the Brownian motion force and the connector force respectively. From the equation of the motion of a dumbbell and a continuity relationship, one can derive the following evolution equation [7]

$$\frac{4}{\zeta} < F(R)\, \boldsymbol{RR} > + < \overset{\nabla}{\boldsymbol{RR}} > = \frac{4kT}{\zeta}\boldsymbol{I}, \tag{6}$$

where ζ is a drag coefficient.

Now, we have to characterize the connector force law. Although a number of springs can be used, we will consider only the Hookean dumbbell and the Warner force law leading respectively to Oldroyd-B and FENE models.

- Let us first consider that F is just a constant H. One can eliminate $< \boldsymbol{RR} >$ from equations (6) and (5) and obtain an Oldroyd-B fluid with :

$$\boldsymbol{T}_V + \underbrace{\frac{\zeta}{4H}}_{\lambda} \overset{\nabla}{\boldsymbol{T}}_V = \underbrace{\frac{n\zeta kT}{2H}}_{2\eta_V} \boldsymbol{D}. \tag{7}$$

- The Warner force law allows us to avoid the unphysical possibility of infinitely extending dumbbells. In fact, the FENE spring is considered as a non-linear connector described by

$$F(R) = \frac{H}{(1 - R^2/R_0^2)}, \tag{8}$$

where R_0 represents the maximum allowable dumbbell length. The FENE model is characterized by the equations (5) (6) and (8).

- Finally, let us consider the FENE-P model. First, we define a non-dimensional configuration tensor $\boldsymbol{A}$ and a characteristic length R_e as follows,

$$\begin{aligned} \boldsymbol{A} &= \frac{3 < \boldsymbol{RR} >}{R_e^2}, \\ R_e^2 &= \frac{3kT}{F(R_e)}. \end{aligned} \tag{9}$$

Introducing the following Peterlin's approximation:

$$< \frac{H}{(1 - R^2/R_0^2)}\, \boldsymbol{RR} >= \frac{H}{(1 - < R^2 > /R_0^2)} < \boldsymbol{RR} >$$

in (6) and taking advantage of (9), we obtain the following equations which govern respectively the fields $\boldsymbol{A}$ and $\boldsymbol{T}_V$:

$$\begin{aligned} \boldsymbol{A} + \lambda\,(1 - tr\boldsymbol{A}/L^2)\, \overset{\nabla}{\boldsymbol{A}} &= \left(\frac{1 - tr\boldsymbol{A}/L^2}{1 - 3/L^2}\right)\boldsymbol{I}, \\ \boldsymbol{T}_V &= \eta_V/\lambda \left(\frac{1}{1 - tr\boldsymbol{A}/L^2}\right)\left(\boldsymbol{A} - \frac{1 - tr\boldsymbol{A}/L^2}{1 - 3/L^2}\boldsymbol{I}\right). \end{aligned} \tag{10}$$

where $L^2 = 3R_0^2/R_e^2$ is a measure of the extensibility of the dumbbells. The relaxation time and the zero-shear viscosity are defined by:

$$\lambda = \frac{\zeta}{4H}, \quad \eta_V = \frac{n\zeta kT}{4H}(1 - 3/L^2). \tag{11}$$

The equations 10 exhibit stable numerical properties and appear to be very useful for the numerical calculations. Chilcott and Rallison [9] introduced some further modification in the evolution equation for $\boldsymbol{A}$ in order to obtain a fluid with a constant viscosity in steady shear flow:

$$\boldsymbol{A} + \lambda\,(1 - tr\boldsymbol{A}/L^2)\,\overset{\triangledown}{\boldsymbol{A}} = \boldsymbol{I}. \tag{12}$$

2.3 Quasi-Linear Equations and Characteristics

In order to analyze the change of type, let us use the following generic block-tensor notation introduced in [1] [10] :

$$A_{ijK}(X)\partial_K X_j = B_i(X), \tag{13}$$

where $X = (X_1, X_2, \ldots)$ is the set of unknowns. Each component X_j, A_{ijK} and B_i may be scalar, vector or tensor. The capital indice K vary from 1 to 4 in three-dimensional case and denotes a component of space-time coordinates. Summation on repeated indices is used and the symbol ∂_K stands for a partial derivation in the appropriate space or time. In other words, ∂_K can be defined as $(\boldsymbol{\nabla}, \partial_t)$.

Equations (13) are equivalent to the formulation

$$\forall \widehat{X}_i, \quad \underbrace{\widehat{X}_i A_{ijK}(X)\partial_K X_j}_{\mathcal{F}(X_j, \widehat{X}_i, X, \partial_K)} = \widehat{X}_i B_i(X), \tag{14}$$

where $\mathcal{F}(X_i, \widehat{X}_j, X, \partial_K)$ is a bilinear form.

Let us now recall that a space-time hypersurface is characteristic in a point when the partial derivatives of the unknowns in the normal direction cannot be obtained from the equations and the values of the unknowns on the hypersurface. If the direction e_K is a characteristic direction, i.e. the normal to the characteristic hypersurface, the form $\mathcal{F}(\partial_e X_j, \widehat{X}_i, X, e_K)$ degenerates, because the system to solve in $X_j^* = \partial_e X_j$ is then singular. This is equivalent to the condition :

$$\begin{aligned} &\exists \widehat{X}_i \quad \text{such that} \\ &\forall X_j^*, \quad \underbrace{\widehat{X}_i A_{ijK}(X) e_K X_j^*}_{\mathcal{F}(X_j^*, \widehat{X}_i, X, e_K)} = 0, \end{aligned} \tag{15}$$

Such a condition (15) can be conveniently written in terms of the determinant $\mathcal{R}(e_K, X)$ of the form $\mathcal{F}$. This determinant needs to be factorized, in order to distinguish between the different characteristic hypercone sheets. This hypercone is defined by the envelope of all characteristic hypersurfaces passing through a fixed point $\boldsymbol{x}^*$ at some t^*. The generating lines of the hypercone sheets are the set ξ_K space-time bicharacteristic directions :

$$\xi_K = \frac{\partial \mathcal{R}}{\partial e_K} \tag{16}$$

Infinitesimal waves originating from ($\boldsymbol{x}^*$,t^*) propagate in the ξ_K direction. The system (13) is evolutionary when the intersection of each characteristic cone sheet with the hyperplane $t = constant$ is a single point. Physically, a non evolutionary problem corresponds to infinitesimal waves propagating at an infinite velocity or in negative time directions. This situation is sketched in Fig.1c

Wave propagation is subcritical or supercritical depending on whether the intersection of the dual hypercone generated by the set of e_K characteristic directions with the same hyperplane is or is not limited to a single point, as shown in Fig.1a and Fig.1b. For a steady-state problem, the set of equations changes type when the associted transient problem changes from subcritical to supercritical.

3 Characteristic Sheets of a FENE-P Fluid

In the absence of body forces and Newtonian extra-stresses, the mass, momentum and constitutive equations of a FENE-P fluid are written as follows :

$$\begin{aligned} \boldsymbol{A} + \lambda(1 - tr\boldsymbol{A}/L^2) \overset{\nabla}{A} - \frac{1 - tr\boldsymbol{A}/L^2}{1 - 3/L^2}\boldsymbol{I} &= 0, \\ \frac{\eta_V}{\lambda}\boldsymbol{\nabla} \cdot \left(\frac{1}{1 - tr\boldsymbol{A}/L^2}\boldsymbol{A} - \frac{1}{1 - 3/L^2}\boldsymbol{I} \right) - \boldsymbol{\nabla} p - \rho \frac{D\boldsymbol{v}}{Dt} &= 0, \\ \boldsymbol{\nabla} \cdot \boldsymbol{v} &= 0. \end{aligned} \tag{17}$$

The weak formulation of equations (17) may be written in the generic formulation (14)

with the set of unknowns X defined as $(\boldsymbol{A}, \boldsymbol{v}, p)$.

$$
\begin{aligned}
\forall \widehat{X}_i, \qquad & \widehat{\boldsymbol{X}}_1 : \Big[\lambda(1 - tr\boldsymbol{A}/L^2)\ (\partial_t + \boldsymbol{v}\cdot\boldsymbol{\nabla})\,\boldsymbol{X}_1 \\
& \qquad -\lambda(1 - tr\boldsymbol{A}/L^2)\left((\boldsymbol{\nabla}\boldsymbol{X}_2)^T\cdot\boldsymbol{A} + \boldsymbol{A}\cdot\boldsymbol{\nabla}\boldsymbol{X}_2)\right)\Big] \\
& + \widehat{\boldsymbol{X}}_2 \cdot \Big[-\frac{\eta_V}{\lambda(1 - tr\boldsymbol{A}/L^2)}\boldsymbol{\nabla}\cdot\boldsymbol{X}_1 - \frac{\eta_V}{\lambda L^2(1 - tr\boldsymbol{A}/L^2)^2}\boldsymbol{\nabla}(\boldsymbol{I} : \boldsymbol{X}_1)\cdot\boldsymbol{A} \\
& \qquad + \rho\,(\partial_t + \boldsymbol{v}\cdot\boldsymbol{\nabla})\,\boldsymbol{X}_2 + \boldsymbol{\nabla}X_3\Big] \\
& + \widehat{X}_3\ \boldsymbol{\nabla}\cdot\boldsymbol{X}_2 \\
& = \widehat{\boldsymbol{X}}_1 : \left[\frac{1 - tr\boldsymbol{A}/L^2}{1 - 3/L^2}\boldsymbol{I} - \boldsymbol{A}\right]
\end{aligned}
\tag{18}
$$

where $\widehat{\boldsymbol{X}_1}$ and $\boldsymbol{X}_1$ are symmetric.

Therefore, the characteristic directions $e_K = (e_x, e_y, e_z, e_t)$ can be obtained by the degeneration condition (15). Hence, $X_j^* = \partial_e X_j$ must be substitued for X_j and e_k for ∂_k when applying the definition of the bilinear form $\mathcal{F}$.

$$
\begin{aligned}
\exists \widehat{X}_i \qquad & \text{such that} \\
\forall X_j^*, \qquad & \widehat{\boldsymbol{X}}_1 : \Big[\lambda(1 - tr\boldsymbol{A}/L^2)\ \ \phi\boldsymbol{X}_1^* \\
& \qquad -\lambda(1 - tr\boldsymbol{A}/L^2)\left((\boldsymbol{X}_2^*\ \boldsymbol{A}\cdot\boldsymbol{e} + \boldsymbol{e}\cdot\boldsymbol{A}\ \boldsymbol{X}_2^*)\right)\Big] \\
& + \widehat{\boldsymbol{X}}_2 \cdot \Big[-\frac{\eta_V}{\lambda(1 - tr\boldsymbol{A}/L^2)}\ \boldsymbol{e}\cdot\boldsymbol{X}_1^* \\
& \qquad -\frac{\eta_V}{\lambda L^2(1 - tr\boldsymbol{A}/L^2)^2}\ \boldsymbol{e}\cdot\boldsymbol{A}\ \boldsymbol{I} : \boldsymbol{X}_1^* \\
& \qquad +\rho\phi\ \boldsymbol{X}_2^* + \boldsymbol{e}X_3^*\Big] \\
& + \widehat{X}_3\ \boldsymbol{e}\cdot\boldsymbol{X}_2^* = 0
\end{aligned}
\tag{19}
$$

where the symbols $\boldsymbol{e}$ and ϕ are defined by :

$$
\begin{aligned}
\boldsymbol{e} &= (e_x, e_y, e_z), \\
\phi &= \boldsymbol{v}\cdot\boldsymbol{e} + e_t
\end{aligned}
\tag{20}
$$

Finally, after some manipulations on condition (19), one finds :

$$
\begin{aligned}
&\exists \widehat{X}_i \qquad \text{such that} \\
&\forall X_j^*, \qquad \boldsymbol{X}_1^* : \Big[\lambda(1-tr\boldsymbol{A}/L^2)\ \phi\widehat{\boldsymbol{X}}_1 - \frac{\eta_V}{\lambda(1-tr\boldsymbol{A}/L^2)}\,\widehat{\boldsymbol{X}}_2\,\boldsymbol{e} \\
&\qquad\qquad -\frac{\eta_V}{\lambda L^2(1-tr\boldsymbol{A}/L^2)^2}\,\boldsymbol{e}\cdot\boldsymbol{A}\cdot\widehat{\boldsymbol{X}}_2\,\boldsymbol{I}\Big] \\
&\quad + \boldsymbol{X}_2^*\cdot\Big[\rho\phi\widehat{\boldsymbol{X}}_2 + \boldsymbol{e}\widehat{X}_3 \\
&\qquad\qquad -\lambda(1-tr\boldsymbol{A}/L^2)\Big((\widehat{\boldsymbol{X}}_1\cdot\boldsymbol{A}\cdot\boldsymbol{e}+\boldsymbol{e}\cdot\boldsymbol{A}\cdot\widehat{\boldsymbol{X}}_1)\Big)\Big] \\
&\quad - X_3^*\Big[\boldsymbol{e}\cdot\widehat{\boldsymbol{X}}_2\Big] = 0
\end{aligned}
\tag{21}
$$

This degeneration condition states that $(\boldsymbol{e}, e_t)$ is a characteristic direction if the form vanishes for some $(\widehat{\boldsymbol{X}}_1, \widehat{\boldsymbol{X}}_2, \widehat{X}_3)$ and for all $\boldsymbol{X}_1^*$, $\boldsymbol{X}_2^*$ and X_3^*. Then, it is easy to develop a complete discussion of the characteristic hypercone sheets. Fig.2 illustrates the results for the 2-dimensional case.

- **Incompressibility sheet**
  If $\boldsymbol{e} = 0$ and $e_t \neq 0$, non trivial solutions with $\widehat{\boldsymbol{X}}_1 = 0$ and $\widehat{\boldsymbol{X}}_2 = 0$ proves the existence of incompressibility waves. The characteristic sheet is a whole $t = constant$ hyperplane.

- **Pathlines sheet**
  If $\phi = 0$ and $\boldsymbol{e} \neq 0$, non trivial solutions with $\widehat{\boldsymbol{X}}_2 = 0$ may be found. The characteristic is well known and reduces to a space-time pathline direction.

- **Shear waves sheet**
  Suppose now that $\phi \neq 0$ and $\boldsymbol{e} \neq 0$. Degeneration of the form $\mathcal{F}$ occurs only if the symmetric tensorial factor of $\boldsymbol{X}_1^*$, the vectorial factor of $\boldsymbol{X}_2^*$ and the scalar vector of

X_3^* vanish simultaneously in condition (21). This leads to the following equations :

$$\begin{aligned}
&\lambda(1-tr\boldsymbol{A}/L^2)\ \phi\widehat{\boldsymbol{X}}_1 - \frac{\eta_V}{\lambda(1-tr\boldsymbol{A}/L^2)}\ \widehat{\boldsymbol{X}}_2\boldsymbol{e} \\
&\qquad -\frac{\eta_V}{\lambda L^2(1-tr\boldsymbol{A}/L^2)^2}\ \boldsymbol{e}\cdot\boldsymbol{A}\cdot\widehat{\boldsymbol{X}}_2\ \boldsymbol{I} = 0 \\
&\rho\phi\widehat{\boldsymbol{X}}_2 + \boldsymbol{e}\widehat{X}_3 \\
&\qquad -\lambda(1-tr\boldsymbol{A}/L^2)\left((\widehat{\boldsymbol{X}}_1\cdot\boldsymbol{A}\cdot\boldsymbol{e} + \boldsymbol{e}\cdot\boldsymbol{A}\cdot\widehat{\boldsymbol{X}}_1)\right) = 0 \\
&\boldsymbol{e}\cdot\widehat{\boldsymbol{X}}_2\ = 0
\end{aligned} \tag{22}$$

Neglecting the trivial case $\lambda = 0$, one obtains from equation (22.1) :

$$\begin{aligned}
\widehat{\boldsymbol{X}}_1 = &\frac{\eta_V}{\lambda^2\phi(1-tr\boldsymbol{A}/L^2)^2}\ \widehat{\boldsymbol{X}}_2\boldsymbol{e} \\
&+\frac{\eta_V}{\lambda^2\phi L^2(1-tr\boldsymbol{A}/L^2)^3}\ \boldsymbol{e}\cdot\boldsymbol{A}\cdot\widehat{\boldsymbol{X}}_2\ \boldsymbol{I}
\end{aligned} \tag{23}$$

Multiplying (22.2) by $\boldsymbol{e}$ and taking advantage of (23), (22.3), we also write :

$$\begin{aligned}
\widehat{X}_3 = &\left(\frac{\eta_V}{\lambda\phi(1-tr\boldsymbol{A}/L^2)}\right. \\
&\left.+\frac{2\eta_V}{\lambda\phi L^2(1-tr\boldsymbol{A}/L^2)^2}\ \frac{\boldsymbol{e}\cdot\boldsymbol{A}\cdot\boldsymbol{e}}{\boldsymbol{e}\cdot\boldsymbol{e}}\right)\boldsymbol{e}\cdot\boldsymbol{A}\cdot\widehat{\boldsymbol{X}}_2
\end{aligned} \tag{24}$$

Finally, equation (22.2) is satisfied if the products by the vectors $\widehat{\boldsymbol{X}}_2$ and $\boldsymbol{e}\times\widehat{\boldsymbol{X}}_2$ respectively are zero. It is clear that a vanishing $\widehat{\boldsymbol{X}}_2$ cannot be considered. The second product yields an identity, and the first one gives the following condition $\mathcal{R}(\boldsymbol{e},\phi,\boldsymbol{A}) = 0$:

$$\begin{aligned}
&\frac{\eta_V}{\lambda(1-tr\boldsymbol{A}/L^2)}\ \boldsymbol{e}\cdot\boldsymbol{A}\cdot\boldsymbol{e} \\
&\underbrace{\qquad +\frac{2\eta_V}{\lambda L^2(1-tr\boldsymbol{A}/L^2)^2}\ \boldsymbol{e}\cdot\boldsymbol{A}\cdot\boldsymbol{A}\cdot\boldsymbol{e} - \rho\phi^2 = 0}_{\mathcal{R}(\boldsymbol{e},\phi,\boldsymbol{A})}
\end{aligned} \tag{25}$$

3.1 Evolution Condition for a FENE-P Fluid

First, let us define the tensor :

$$\boldsymbol{T}_A\ =\ \frac{\eta_V}{\lambda(1-tr\boldsymbol{A}/L^2)}\ \boldsymbol{A} + \frac{2\eta_V}{\lambda L^2(1-tr\boldsymbol{A}/L^2)^2}\ \boldsymbol{A}\cdot\boldsymbol{A} \tag{26}$$

Note that as the ratio L goes to infinity, the FENE-P fluid is only an Maxwell fluid and one obtains the following expression of this stress tensor :

$$\boldsymbol{T}_A = \frac{\eta_V}{\lambda}\boldsymbol{A} = \boldsymbol{T}_V + \frac{\eta_V}{\lambda}\boldsymbol{I}$$

It is exactly the same expression than the stress tensor defined by Dupret and Marchal [1]. If the positive-definiteness of the tensor $\boldsymbol{T}_A$ is lost, the problem becomes non evolutionary. The expression (26) is also valid for the flow of a Chilcott Rallison fluid.

3.2 Change of Type for a FENE-P Fluid

On one hand, let us define the tensor :

$$\boldsymbol{T}_B = \boldsymbol{T}_A - \rho \boldsymbol{v}\boldsymbol{v} \tag{27}$$

On the other hand, let us consider the steady flow of a FENE-P fluid. The problem is neither purely elliptic neither purely hyperbolic. However, the hyperbolic character of the flow sometimes increases in the sense that it contains additional characteristics other than the streamlines. This happens in the supercritical case. One observes what has been called a *change of type* by Joseph and al. [2]

In order to find a condition for this change of type, we have to consider the solutions $(\boldsymbol{e}, e_t)$ of (25) with a vanishing component e_t. From equations (26) and (25), this leads to the following equation for $\boldsymbol{e}$:

$$\boldsymbol{e} \cdot \boldsymbol{T}_B \cdot \boldsymbol{e} = 0 \tag{28}$$

One can consider both following cases :

- **Subcritical case**
  $\boldsymbol{T}_B$ is positive definite, and equation (28) does not have any solutions. The waves are propagating in all directions.
- **Supercritical case**
  $\boldsymbol{T}_B$ is is not positive definite, and equation (28) has suitable solutions in the hypercone defined by $\boldsymbol{e}$. Let us note that this supercritical case will happen only for fairly non vanishing Reynolds numbers.

4 Numerical Results

Let us now consider the numerical simulation of the flow of aqueous solutions of polyacrylamide in contraction and expansion geometries.

Changes of type described in the previous section can only occur when the fluid is able to exhibit an instantaneous elastic response. However, in order to fit the rheometrical data of the fluid, it is useful to add a small viscous component. Such a Newtonian component also helps the iterative convergence of the numerical calculations. When the retardation time λ^* is small, one may consider that the model with the small viscous component is a singular pertubation and that the validity of the theory is directly related to the magnitude of such a retardation time.

The calculation of the viscoelastic flow is based on the Galerkin formulation of the mixed finite element developed by Marchal and Crochet [3]. Quadrilateral elements are used with linear, quadratic and 4 x 4 linear sub-elements respectively for the pressure, the velocity and the configuration tensor. Converged results are obtained for relatively small values of L^2. However, when L^2 tends to infinity, we have to introduce streamline-upwind technique(SU) for the constitutive equation. Such a technique introduces artificial diffusivity along streamlines. For details about the sensitivity analysis of the numerical parameters of the 4 x 4 SU method, the reader is referred to [11].

The flow is characterized by two dimensionless parameters:

$$We = \frac{\lambda V}{L}, Re = \frac{\rho V L}{\eta_V + \eta_N}, \tag{29}$$

where V is the mean velocity in the narrow channel of height L (or radius, in the axisymmetric case) .

4.1 Planar Four to One Contraction Flows

We first present the planar four-to-one contraction flows. We consider the steady isothermal motion of an incompressible fluid characterized by the FENE-P model. In fact, we are considering the simulation of flows of a 0.25% polyacrylamide aqueous solution described in Purnode and Crochet [4], based on experimental results of Evans and Walters [5] . The material parameters of the FENE-P model are the following :

$$\begin{aligned} L^2 &= 6 \\ \eta_N &= .005\text{Pa s} \\ \eta_V &= .065\text{Pa s} \\ \lambda &= 0.6\text{s} \\ \lambda^* &= 0.043\text{s} \end{aligned}$$

We impose no-slip conditions on the wall, vanishing normal velocity at the plane of symmetry and a fully developed velocity profiles in both entry and exit sections. The configuration tensor is also imposed in the entry section. The lengths of the mesh before and after the contraction are respectively equal to 20 times and 40 times the downstream slit width. A close-up view of the mesh used is shown in Fig.3.

Fig. 4a shows the most significant vortex enhancement features, for increasing values of the Reynolds and Weissenberg numbers. In particular, a lip vortex is created; it then envelops the salient corner vortex, grows in size before being strongly reduced to small remnants. It is interesting to observe that, for high values of We and Re, the streamlines remain unperturbed in the upstream slit, unless close to the contraction plane. It is shown in [4] that this lip vortex enhancement is not a numerical artefact.

In Fig. 4b, the shaded areas correspond to the regions where the tensor $\boldsymbol{T}_B$ loses his positive-definiteness property. In other words, the increase of both We and Re corresponds to an upstream extent of the hyperbolic region: the fluid seems to ignore the discontinuity of the boundary condition at the corner and behaves like in a fully developed flow. Correlation between the change of the type and the lip-vortex mechanism is demonstrated by the comparison of the streamlines of Fig. 4a and the shaded areas of Fig. 4b. In Fig. 5, we also superpose the contourlines of the vorticity to the hyperbolic area. In this closeup view, it is noted that the dark areas seem to correspond to the regions of the hyperbolicity of the vorticity equation. At $We = 4.6$ and $Re = 1.07$, the influence of the vorticity generated at the re-entrant corner extends far upstream. However, for $We = 27.34$ and $Re = 6.37$, this influence is not reaching as far, so that the signal announcing the contraction is not transmitted far upstream.

In this problem, all results presented have Re and We numbers proportional to each other and, hence one should see a way of telling what is related to change of type and what is simply an elastic effect. In order to clarify the point, we take advantage of a suggestion of a referee, and we compare in Fig.6 the result of the numerical simulation with and without inertia. We conclude that inertia and change of type may be responsible for the lip vortex enhancement mechanism.

In order to illustrate the influence of the model, we show in Fig. 7 the most significant features of the flow when L^2 is varied. The streamlines and the hyperbolic regions are shown at $We = 5.83$ and $Re = 1.36$ for L^2 equalling respectively 6, 100 and ∞. Streamline-upwinding is introduced only for the calculations with $L^2 = 100$ and $L^2 = \infty$. It is noted that a large value of L^2 (which is equivalent to an Oldroyd-B fluid) leads both to the upstream increase of the hyperbolic area and to the size reduction of the vortex. This is in line with the expectations and results of Song and Yoo [12] for a UCM fluid using a finite difference technique.

4.2 Tree-Like Jet Flow

In Fig. 8, a polyacrylamide solution flows from a 1mm circular hole into a large reservoir containing the same shear-thinning-elastic liquid. At low flow rates the jet exhibits Newtonian-like fluid behaviour, i.e. just after the expansion plane, the flow is everywhere directed outwards. At higher rates a tree-like flow is observed. The cross-section of the jet does not increase with the distance to the opening until the jet bursts in such a way

that the streamlines are separating like the branches of a tree [6]. Therefore, this flow type is called the *tree-like jet* flow.

We show here numerically that this effect is associated with a change of type of the set of governing equations. The calculations are performed in a 1:140 axisymmetric expansion, this large ratio being a good approximation of a narrow die discharging in a large reservoir. Length of the mesh before and after the expansion are respectively equal to 50 times and 200 times the narrow channel radius. Boundary conditions are no-slip conditions on the wall, vanishing normal velocity on the symmetry axis and a fully developed velocity profiles in both entry and exit sections. Let us recall here that the constitutive equation is integrated by means of the Galerkin method. A closeup view of the mesh is plotted in Fig. 9. We consider here the same fluid data as in the planar contraction case.

In Figs. 10a and 10b, the streamlines and the hyperbolic areas are respectively shown for increasing values of the We and Re. Let us note that, at high values of the dimensionless parameters, the streamlines close to the symmetry axis are not affected by the expansion; this corresponds to a downstream extent of the hyperbolic region.

We also superpose the isovorticity lines and the shaded area in some closeup views in Fig. 11. At $We = 1.73$ and $Re = 1.03$, the vorticity generated at the corner propagates upstream in such a way that the fully developed vorticity profile is perturbed at about 3 radii from the expansion plane. However, at $We = 8.52$ and $Re = 5.09$, the vorticity which is created at the corner, cannot easily propagate its influence in the upstream central region. This is the case of a supercritical flow, where a fluid particle approaching the expansion corner travels with the same vorticity as it had from far upstream as if it did not realize that there is an expansion ahead . It explains the occurence of the bounded jet where its velocity is larger than the speed of the vorticity waves into rest.

In order to illustrate the coupling between inertia an elasticity, we show in Fig.12 the streamlines obtained respectively for the elastic fluid without inertia, the inelastic fluid with inertia and the coupled problem. On one hand, the purely viscoelastic problem without inertia and the same value of the Weissenberg number exhibits a purely elliptic propagation of vorticity. On the other hand, the transport in the inelastic solution is important, but the tree-like flow is not observed. It is quite interesting to note that the tree-like flow is only obtained by the change of type due to the coupling of both inertia and elasticity,

5 Conclusion

A quasi-linear analysis for a FENE-P model has been performed. It appears that a suitable definition of the tensors $\boldsymbol{T}_A$ and $\boldsymbol{T}_B$ allows us to define practical conditions respectively for the loss of evolution and the change of type of the FENE-P model.

We also demonstrate that the numerical simulation is able to reproduce theoretical results of the change of type. Moreover, our numerical results show that typical viscoelastic features can be associated with the change of type of the governing system of equations.

Appendix

We here present the tensorial conditions, expressed in the notation of Bird et al. [7]

$$\boldsymbol{T}_V = \frac{\eta_V}{\lambda}(1+3/b)\left(\frac{1}{(1-tr\boldsymbol{B}/b)}\boldsymbol{B}-\boldsymbol{I}\right),$$

$$\boldsymbol{B}+\lambda(1-tr\boldsymbol{B}/b)\overset{\triangledown}{\boldsymbol{B}}=(1-tr\boldsymbol{B}/b)\boldsymbol{I}.$$

where

- η_V is the zero-shear viscosity
- $\boldsymbol{B} = H < \boldsymbol{RR} > /kT$ is a non-dimensional configuration tensor,
- $b = HR_0^2/kT$ is a measure of the extensibility of the dumbbell,
- R_0 is the maximum allowable length in the Warner law,
- T is the temperature,
- k is the Boltzmann constant.

The tensor $\boldsymbol{T}_A$ is then defined as:

$$\boldsymbol{T}_A = \frac{\eta_V(1+3/b)}{\lambda(1-tr\boldsymbol{B}/b)}\boldsymbol{B} + \frac{2\eta_V(1+3/b)}{\lambda b(1-tr\boldsymbol{B}/b)^2}\boldsymbol{B}\cdot\boldsymbol{B}$$

References

[1] Dupret, F. and Marchal, J.M., J. Méc. Théor. Appl., **5**,403(1986).

[2] Joseph, D.D., Renardy, M., Saut, J.C., Arch. Ration. Mech. Anal., **87**,213(1985).

[3] Marchal,J.M., Crochet,M.J., J. Non-Newt. Fluid Mech.**26**, 77(1987).

[4] Purnode, B., Crochet M.J., submitted for publication(1996).

[5] Evans, R.E., Walters,K., J. Non-Newt. Fluid Mech., **32**,95(1989).

[6] Giesekus, H., Rheol. Acta, **8**,411(1969).

[7] Bird,R.B., Dotson,P.J, Johnson, N.L., J. Non-Newt. Fluid Mech. **7**,213(1980)

[8] Tanner, R.I. *Engineering Rheology*,Clarendon Press, Oxford, 1985

[9] Chilcott, M.D., Rallison, J.M., J. Non-Newt. Fluid Mech. **29**,381(1988).

[10] Dupret, F. and Marchal, J.M., J. Non-Newt. Fluid Mech. **20**,143(1986).

[11] Crochet, M.J., Delvaux, V., Marchal, J.M. J. Non-Newt. Fluid Mech., **34**,261(1990)

[12] Song, J.H., Yoo, J.Y., J. Non-Newt. Fluid Mech., **24**,221(1987).

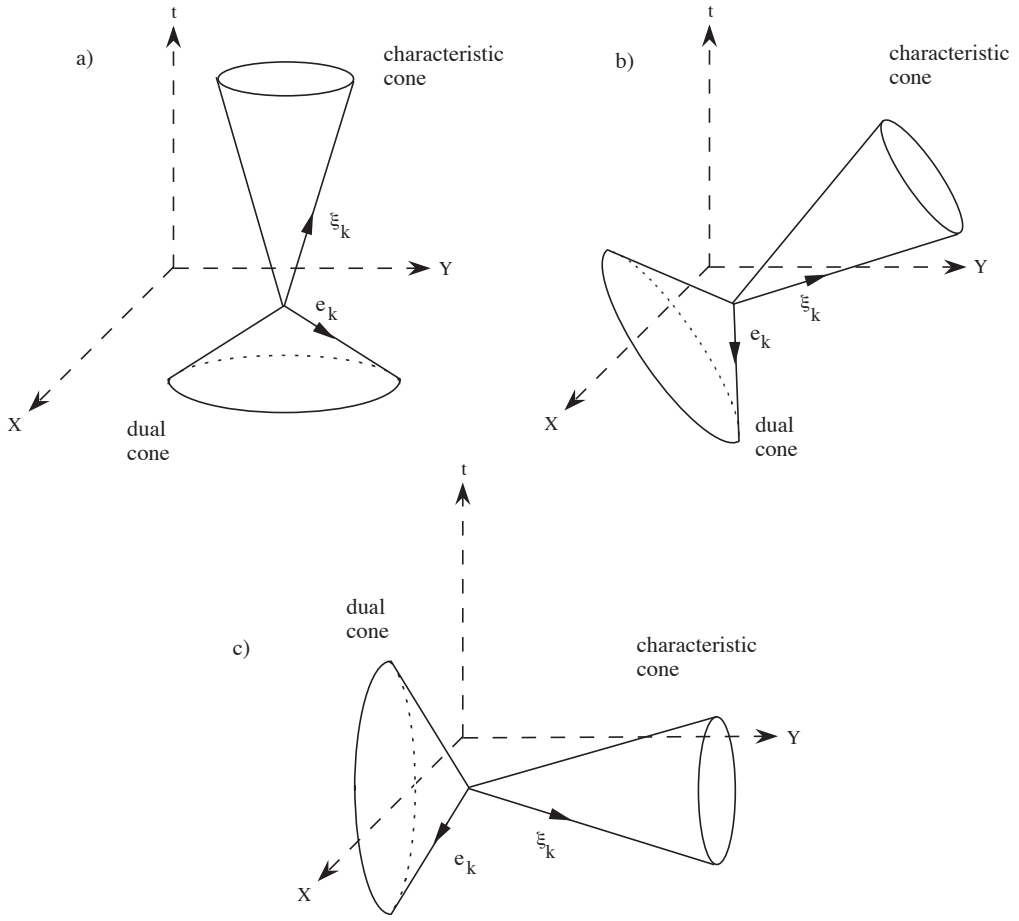

Fig. 1. Characteristic and dual cones: a) subcritical case b) supercritical case c) non-evolutionary case

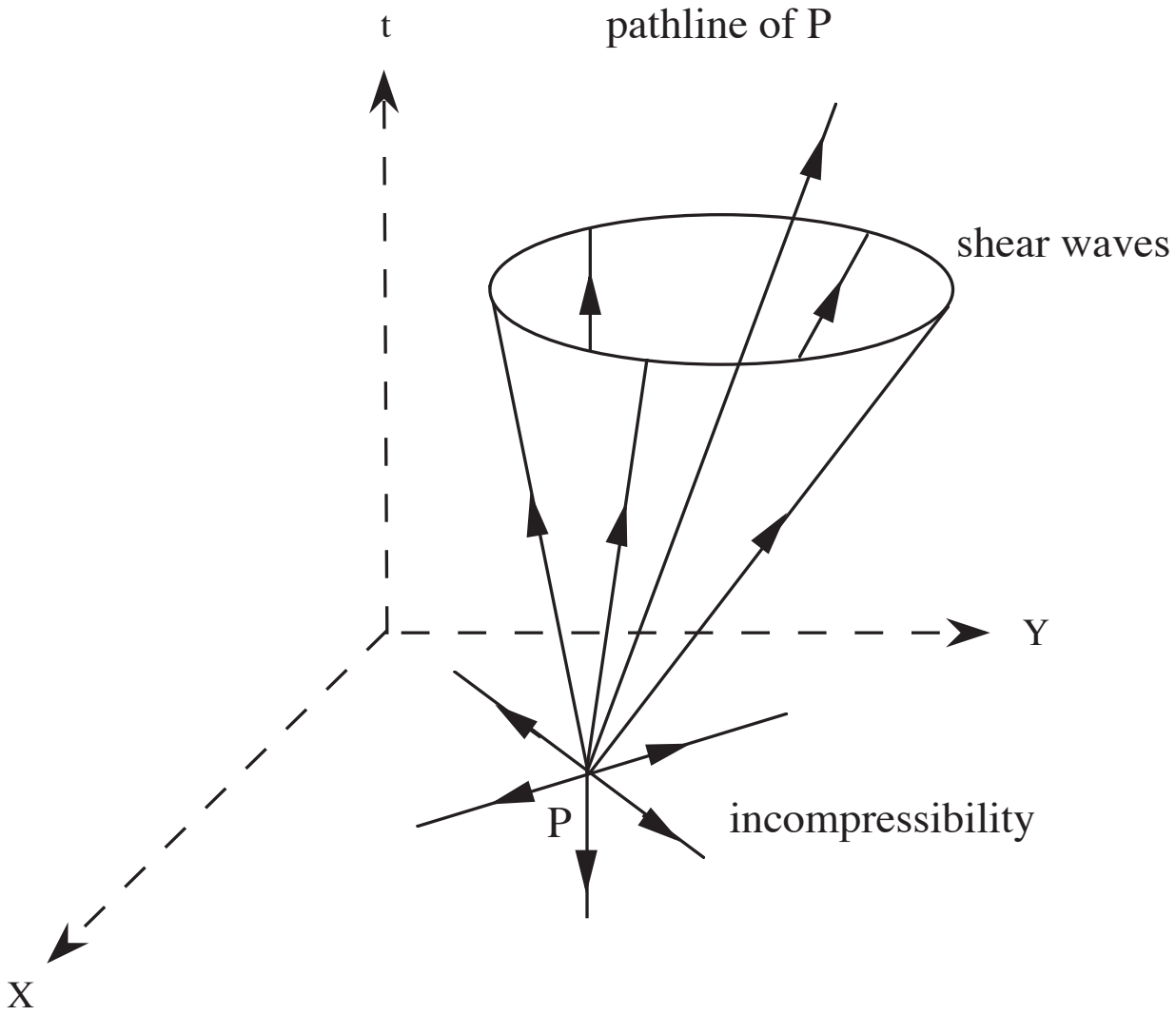

Fig. 2. Characteristic sheets for a transient 2D flow

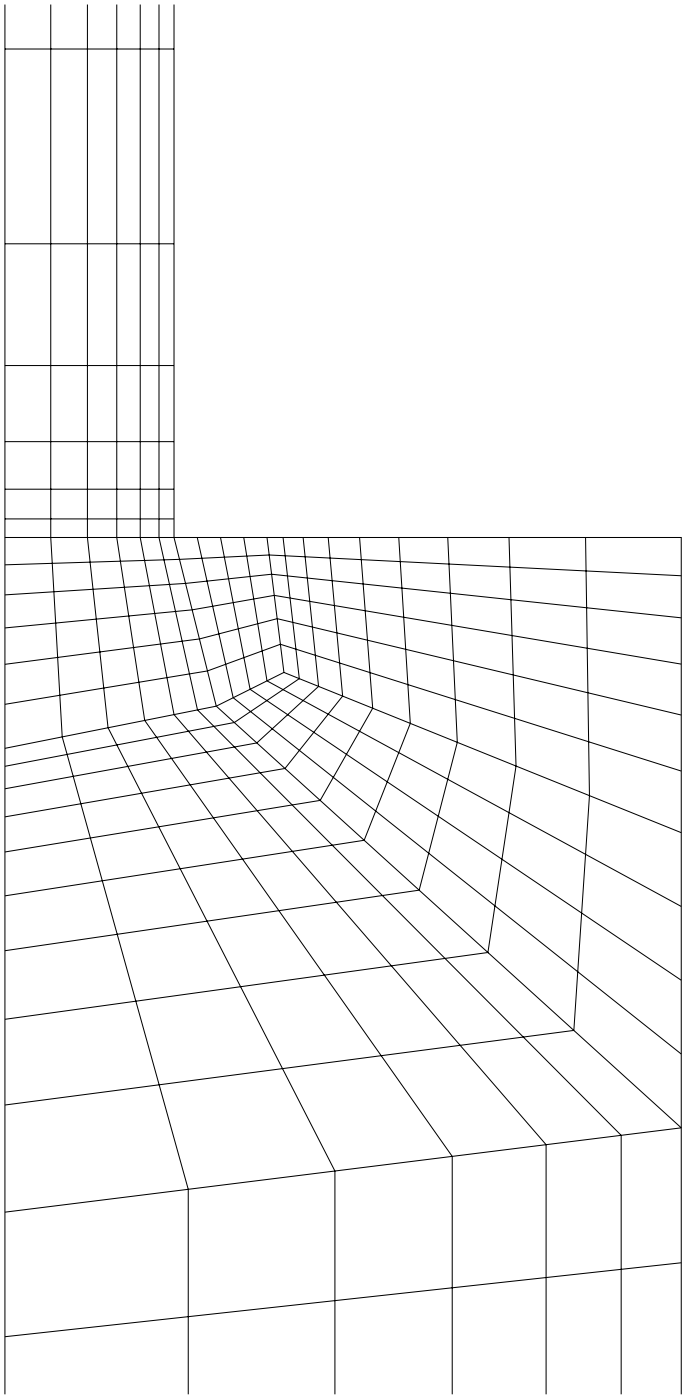

Fig. 3. 4:1 planar contraction: close-up of the finite element mesh

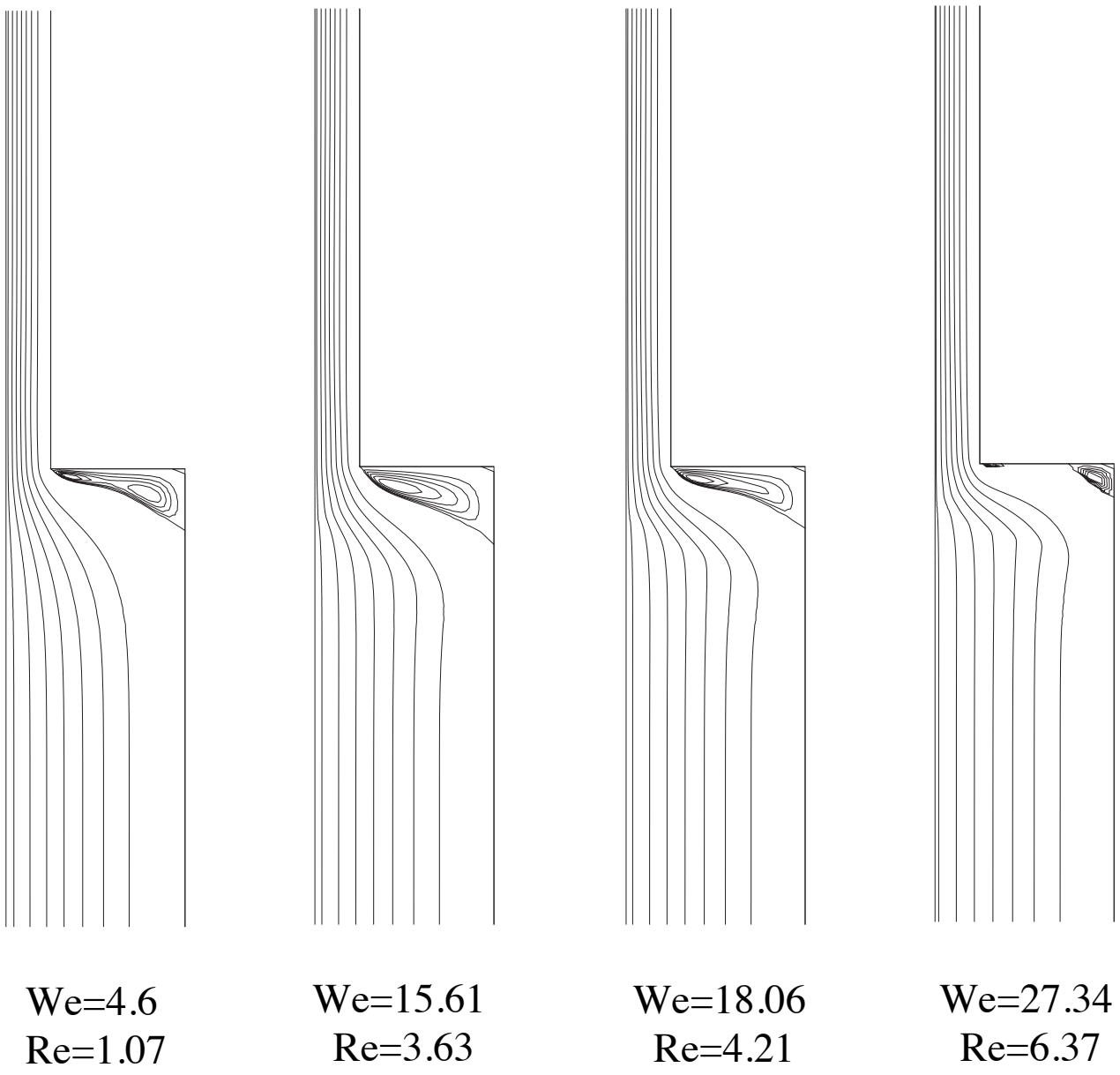

Fig. 4. 4:1 planar contraction of a 0.25% polyacrylamide aqueous solution : a) Streamlines

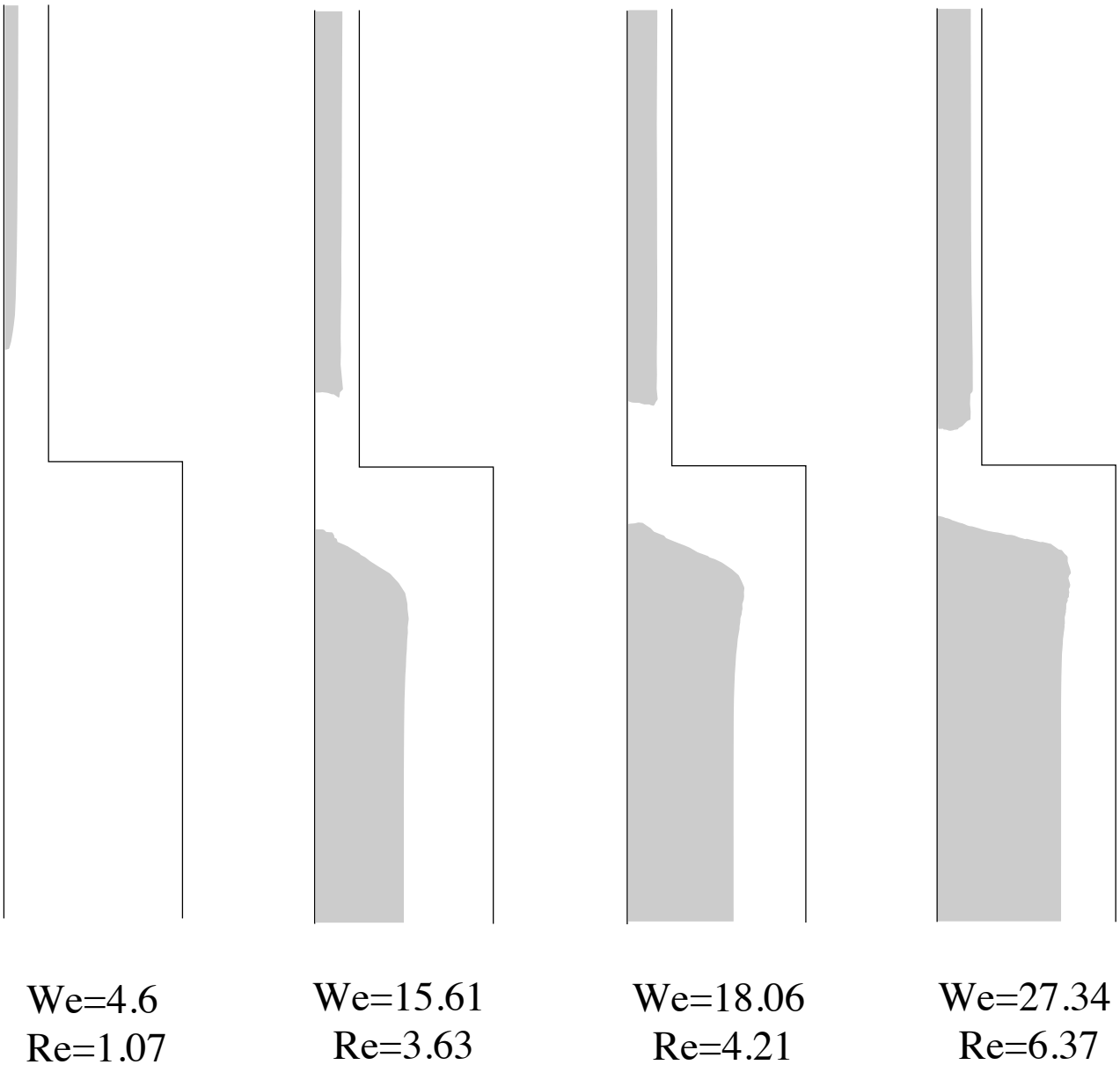

Fig. 4. 4:1 planar contraction of a 0.25% polyacrylamide aqueous solution : b) Hyperbolic flow regions in shaded area

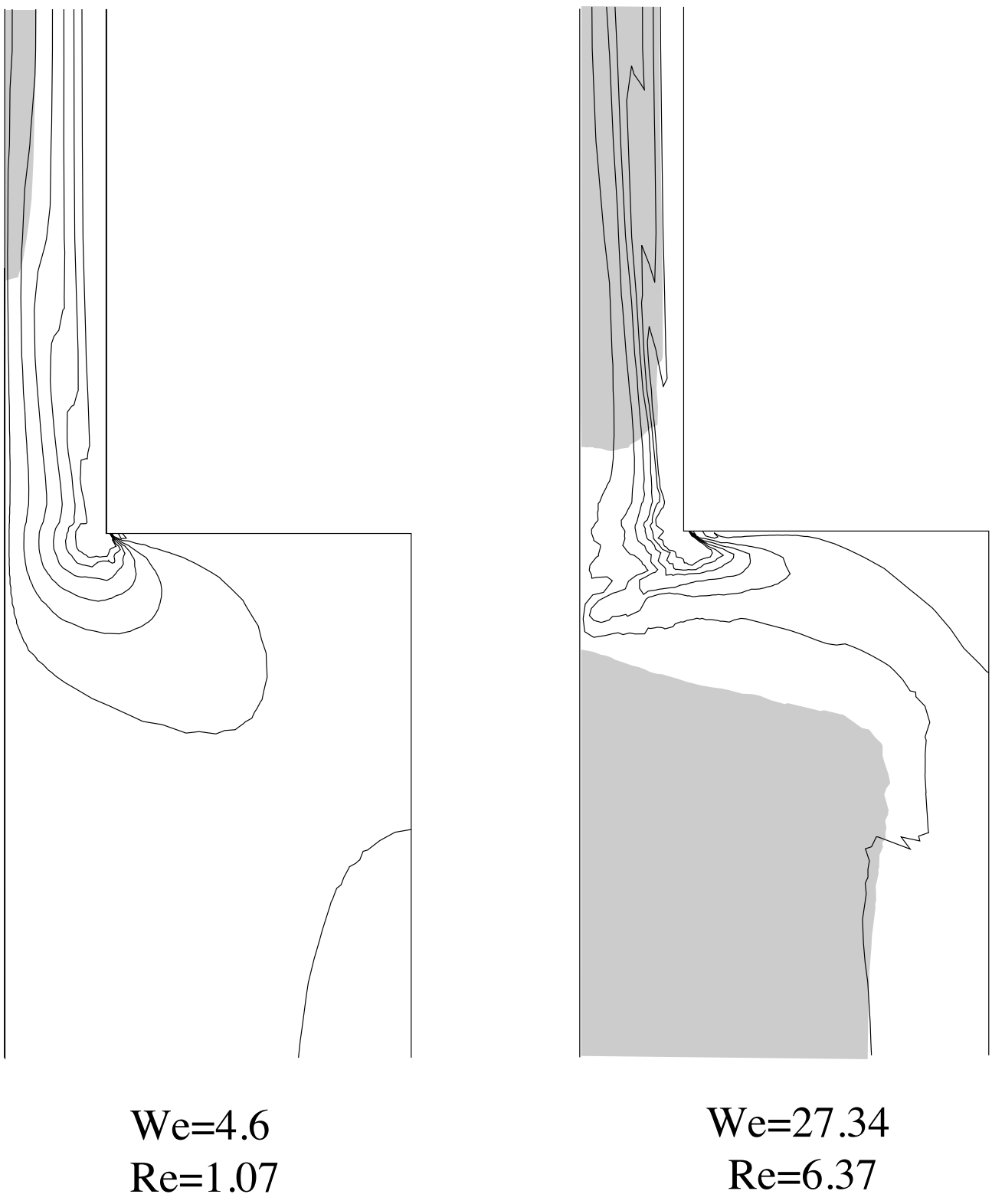

Fig. 5. Comparison of vorticity contourlines and hyperbolic regions

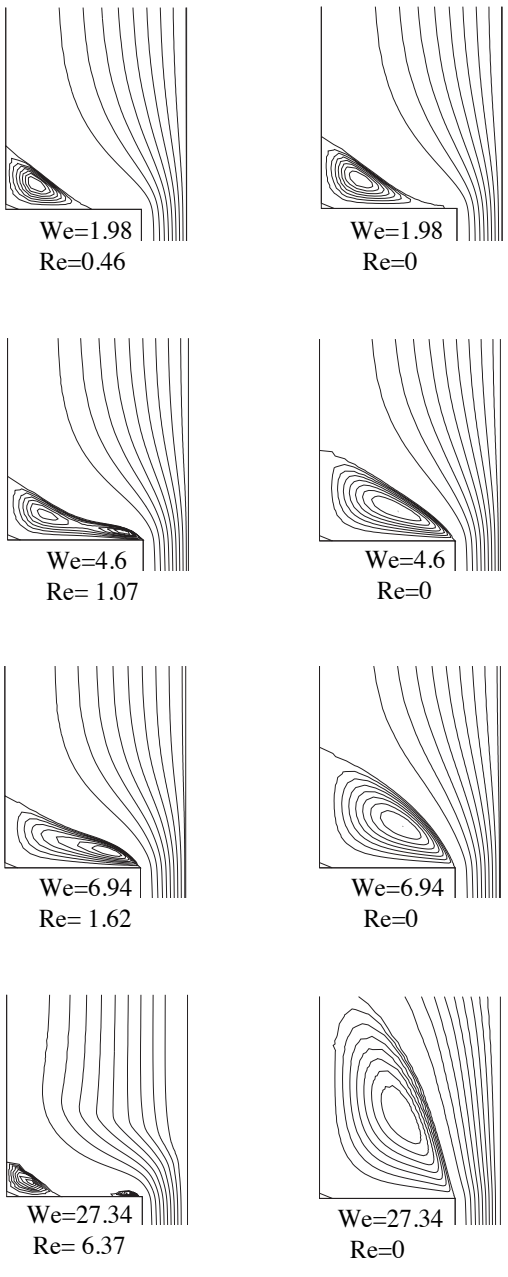

Fig. 6. 4:1 planar contraction of a 0.25% polyacrylamide aqueous solution with inertia effects on the left and without inertia effects on the right.

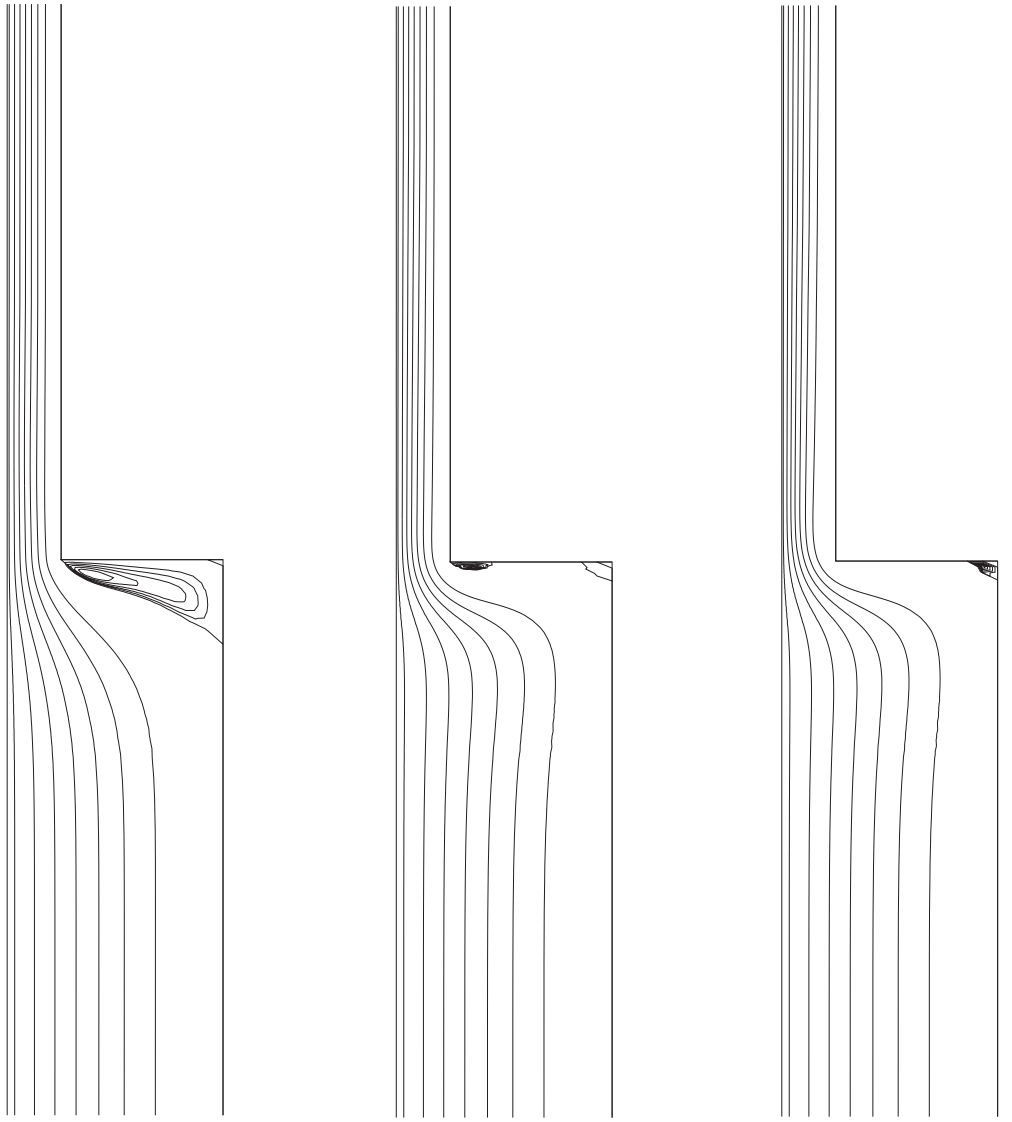

Fig. 7. Effect of L^2 on the flow characteristics: a) Streamlines

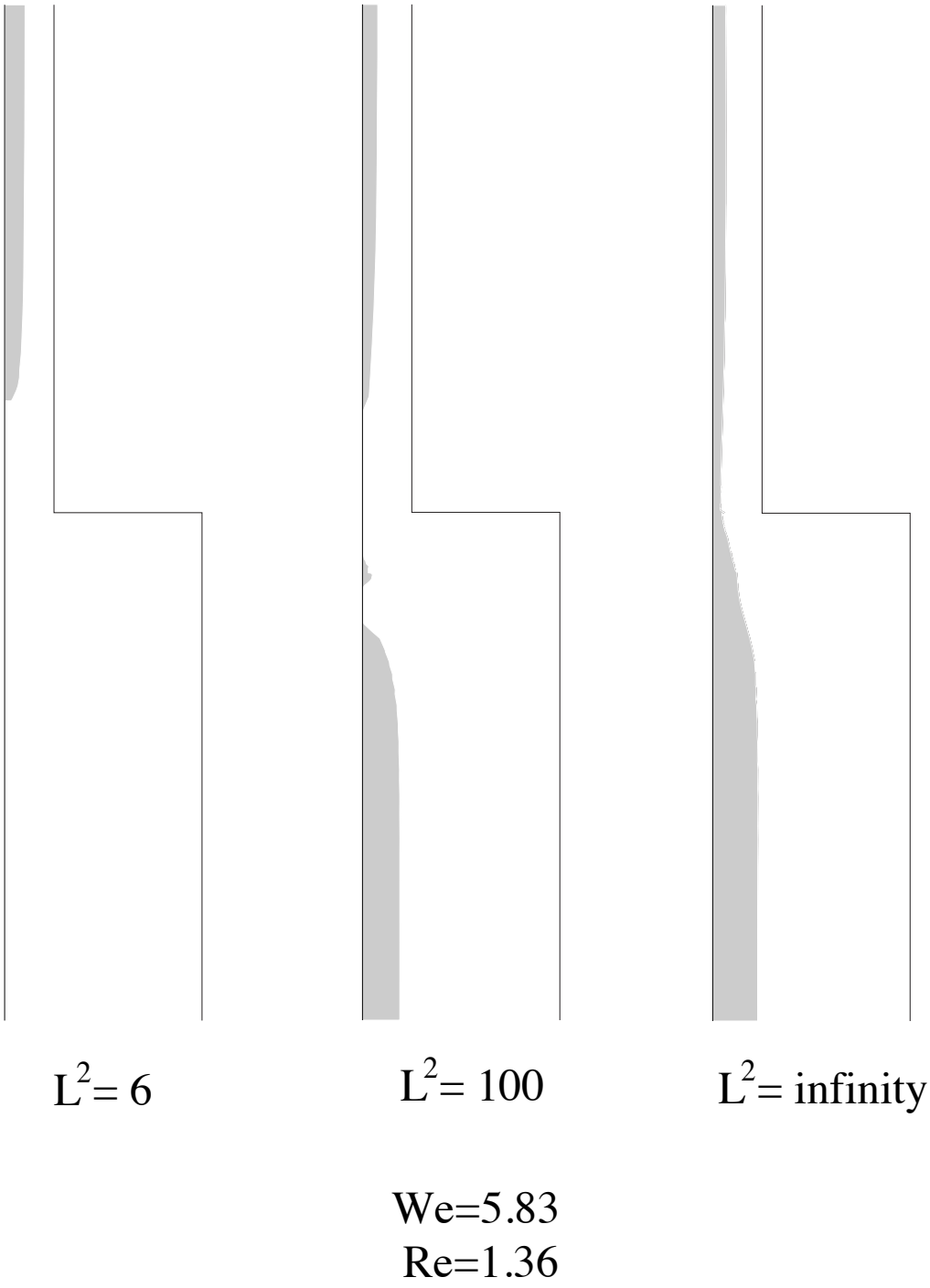

Fig. 7. Effect of L^2 on the flow characteristics: b) Hyperbolic regions in shaded area

Fig. 8. Tree-like jet flow (reprinted from H. Giesekus[6])

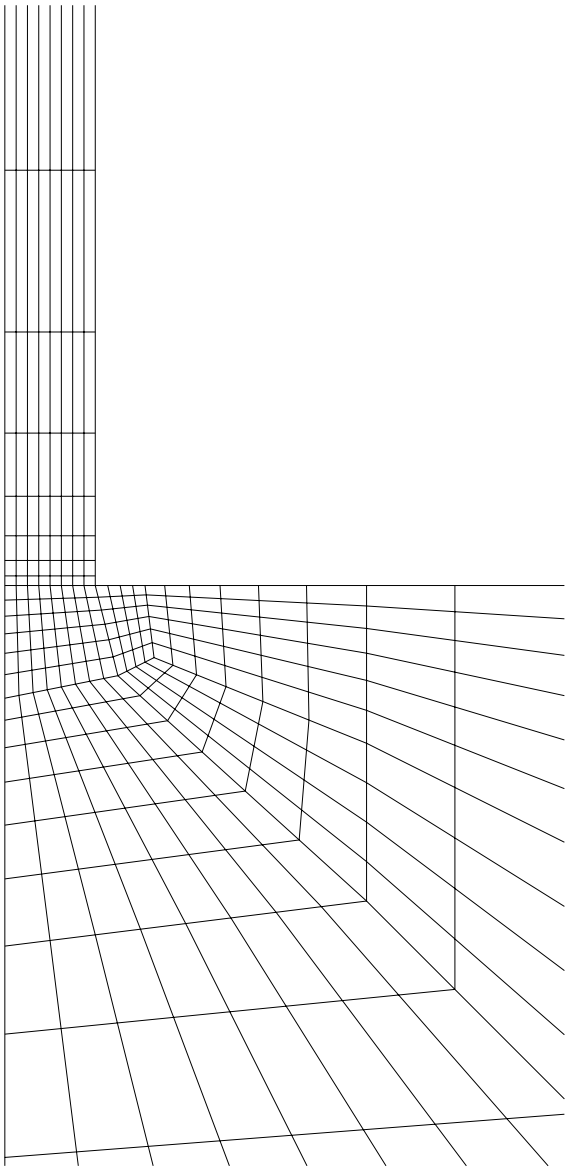

Fig. 9. Finite element mesh used in the simulation of the tree-like jet flow: close-up near the expansion

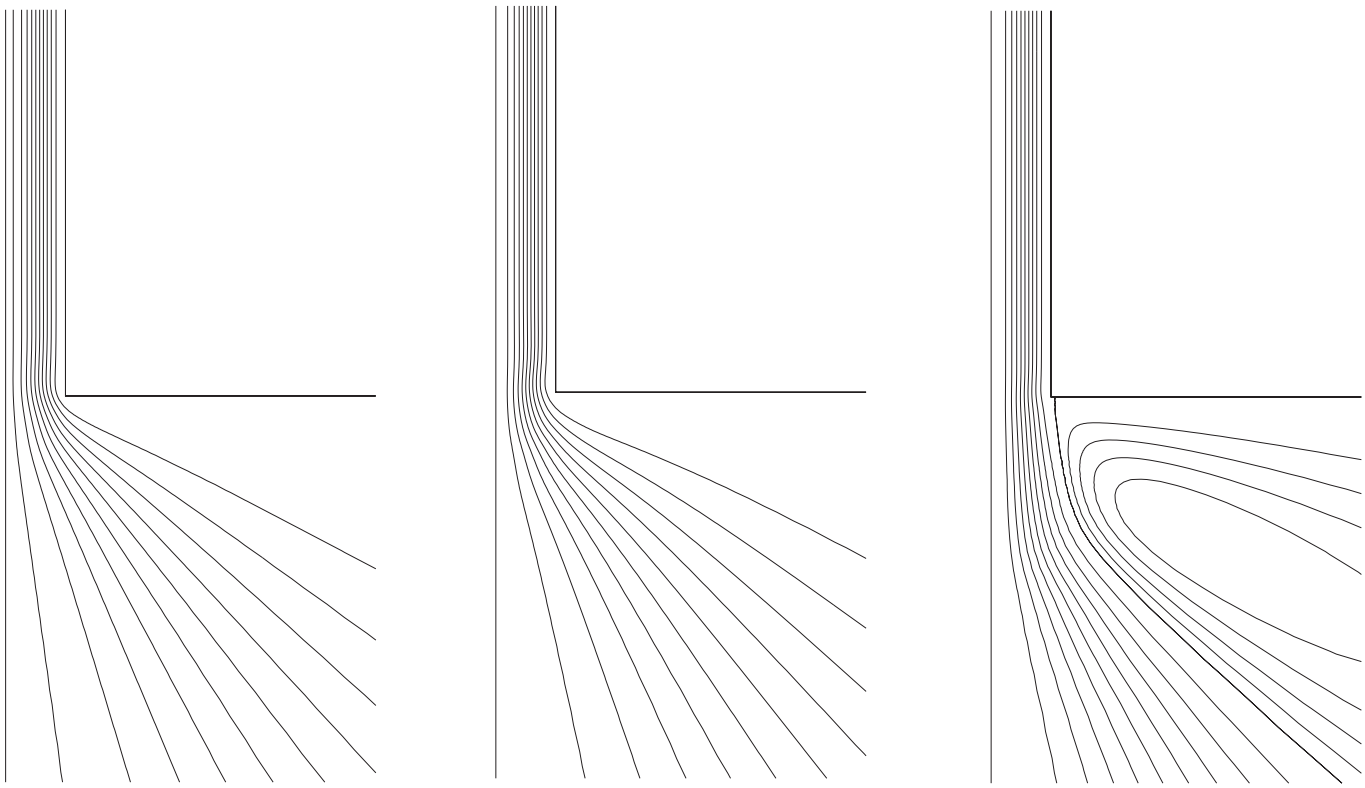

Fig. 10. Expansion flow of a 0.25% polyacrylamide aqueous solution : a) Streamlines

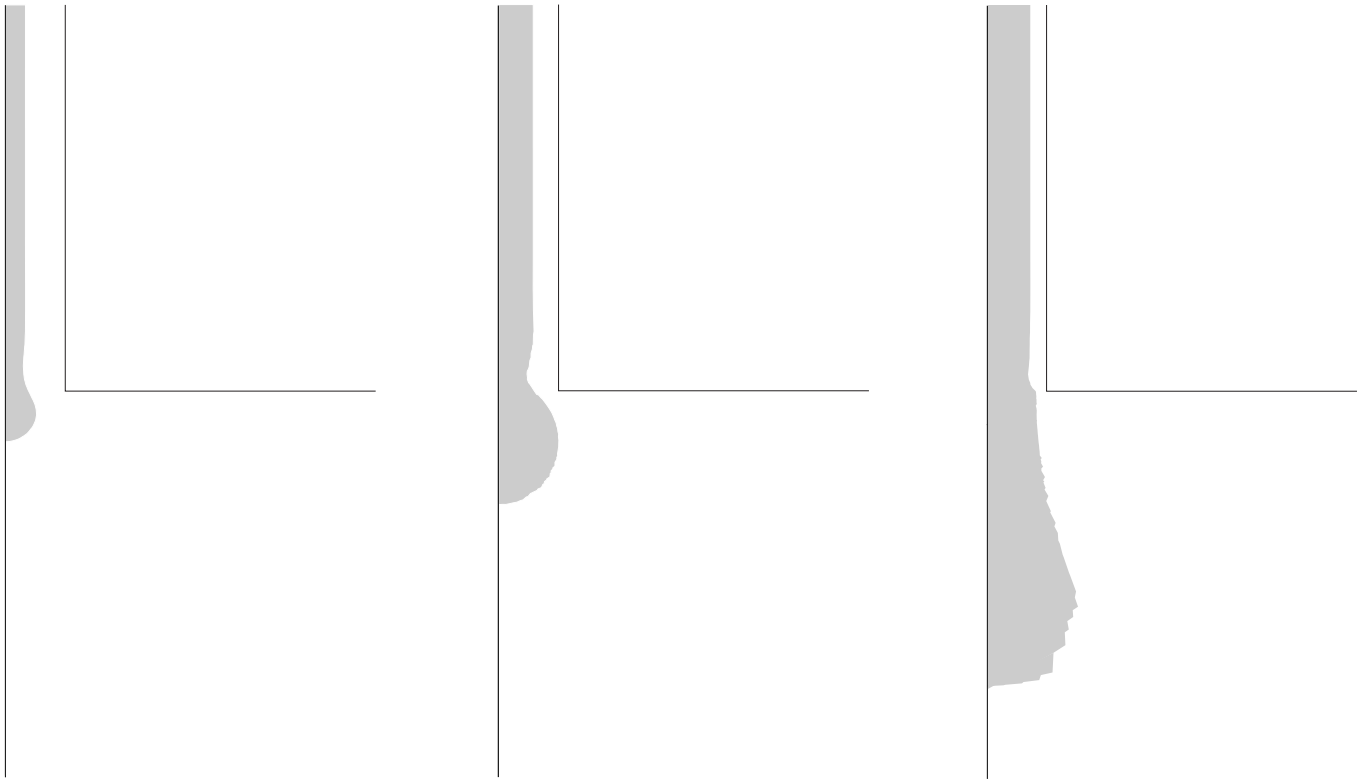

Fig. 10. Expansion flow of a 0.25% polyacrylamide aqueous solution : b) Hyperbolic region in shaded area

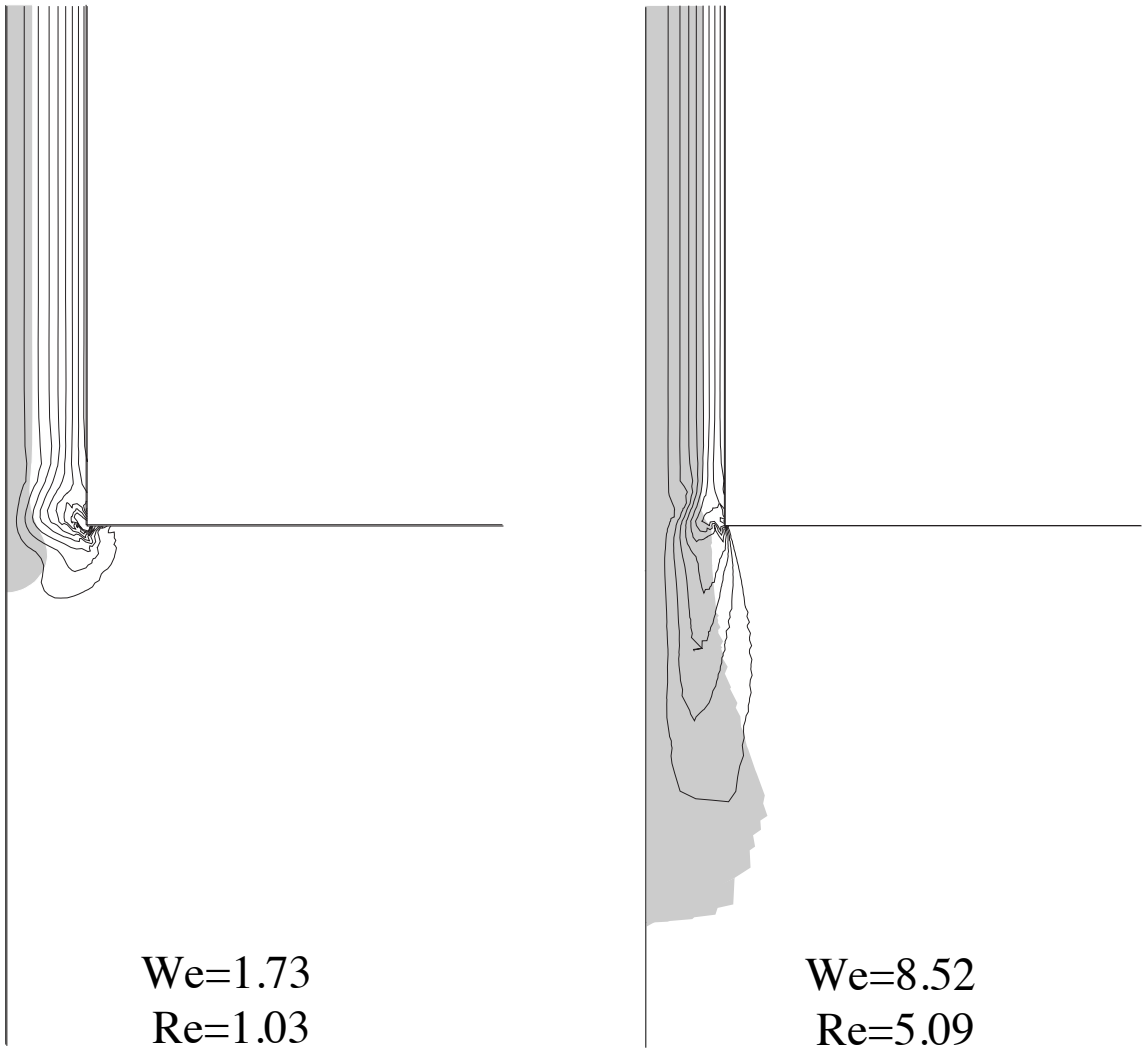

Fig. 11. Expansion flow of a 0.25% polyacrylamide aqueous solution : Comparison of vorticity contourlines and hyperbolic regions

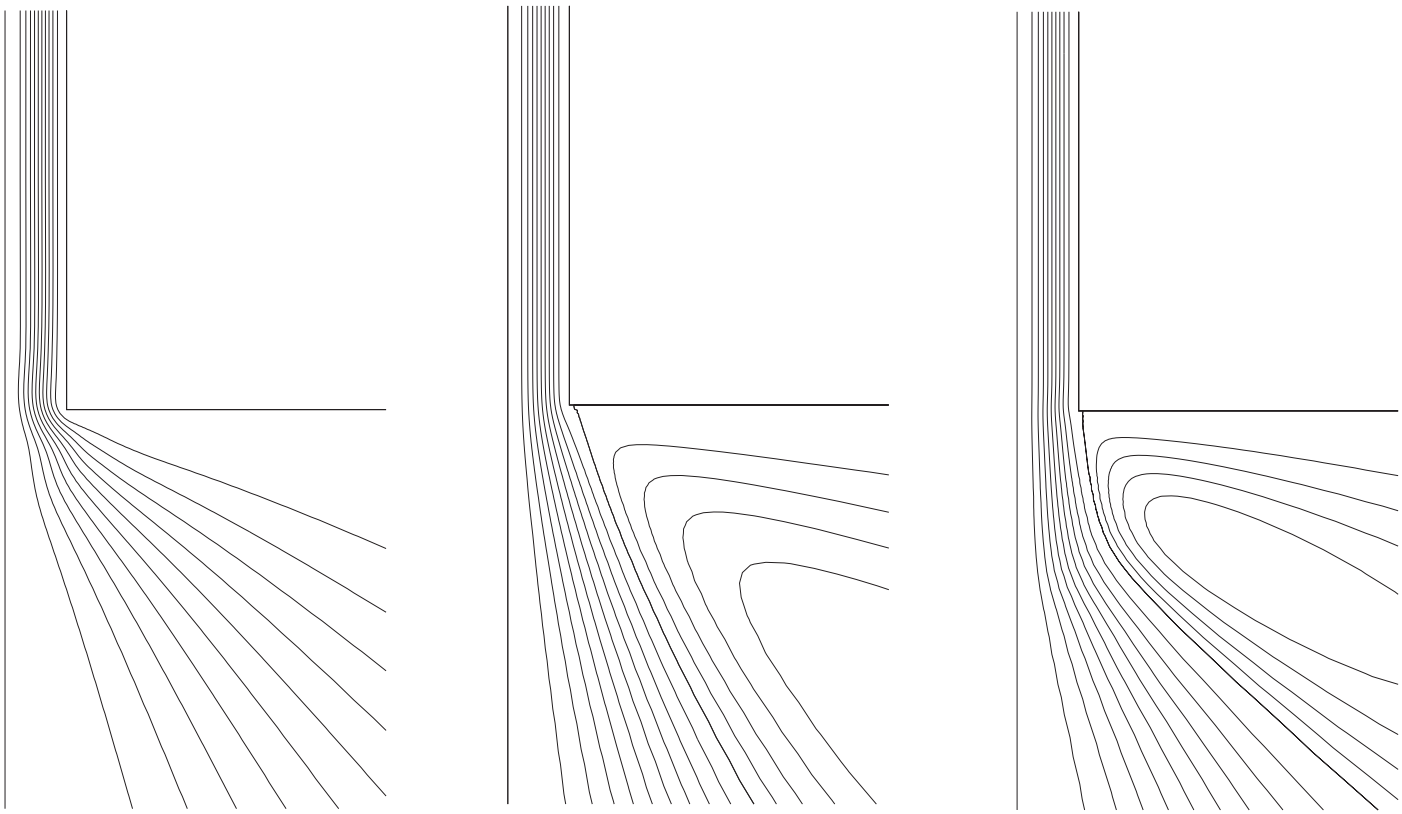

Fig. 12. Expansion flow of a 0.25% polyacrylamide aqueous solution : Comparison between viscoelastic flow without inertia, inelastic flow with inertia and inertial viscoelastic flow

List of Figures